Hindawi
Shock and Vibration
Volume 2022, Article ID 7046036, 15 pages
https://doi.org/10.1155/2022/7046036

Research Article

Influence of Soil-Structure Interaction on the Seismic Response of a Continuous Bridge with Friction Pendulum System

Bing Li,[1] **Chong Fu**,[2] **Guolong Liu**,[1] **Wei Wei**,[1] **Junfa Duan**,[1] **and Bin Wang**[3]

[1]*School of Mechanical Engineering, North China University of Water Resources and Electric Power, Zhengzhou 450045, China*
[2]*Henan Institute of Metrology, Zhengzhou 450008, China*
[3]*Department of Mechanical and Aerospace Engineering, Brunel University London, Uxbridge UB8 3PH, UK*

Correspondence should be addressed to Bin Wang; bin.wang@brunel.ac.uk

Received 6 December 2021; Revised 7 March 2022; Accepted 2 April 2022; Published 22 April 2022

Academic Editor: Nicola Caterino

A three-dimensional finite element analysis was carried out for the influence of soil-structure interaction (SSI) on the seismic response of an isolated continuous bridge with a friction pendulum system (FPS). SSI was modelled using the soil resistance vs deflection nonlinear springs (following *p-y* curves). The influence of SSI on the dynamic behaviour and the seismic response of isolated bridges with different friction coefficients of FPS were investigated using six measured ground motions. Results show that the effect of SSI is limited on the isolation period of the bridge, but significant on the response amplitude of the bridge structures, and particularly on the response amplitude at the pier top and bottom. The displacement and acceleration at the pier top are underestimated, while the shear force and bending moment at the pier bottom are overestimated if the SSI effects are ignored, which suggests that SSI should be considered in the seismic analyses of continuous bridges.

1. Introduction

Vibration and deformation of bridge structures and soil ground foundation are interactive [1, 2]. Theoretical models and analytical methods for lateral load-displacement behaviours of soil adjacent to the bridge piles have been established. According to industry codes for foundation design of railway bridges and culverts [3], SSI can be simulated by the "M" method, in which a series of equivalent linear springs are assumed along the depth of the bridge pile. The soil springs at each depth are calculated using a coefficient of horizontal subgrade reaction that increases linearly with the depth of the bridge pile. For the far-field boundary conditions, Novak and Mitwally [4] proposed a frequency dependent Kelvin element to simulate the infinite soil. In addition, the soil-bridge interaction at the abutment may have a significant effect on the dynamic response characteristics, in particular, for shorter bridges [5]. And it is reported that the interaction between the soil and the abutments should be established in the full bridge model [6, 7].

Non-linear springs based on the well-established soil resistance vs deflection (*p-y*) curves can also be used to represent the load-displacement behaviour of soil adjacent to the piles following the guidelines of industrial codes, e.g., API [8]. Rahmani et al. [7], Wang et al. [9] and Han et al. [10] defined the SSI model according to API rules for different bridge designs, including integral abutment bridges, continuous steel girder bridges and skewed highway bridges. Soneji and Jangid [11] and Mahjoubi and Maleki [12] investigated the influence of SSI on isolated cable-stayed bridges with high-damping rubber bearings (HDRBs), and integral abutment bridges, using direct integration methods and finite element analyses. Their results showed that the nonlinear soil modelling is essential to represent the dynamic behaviour of the soil-pile system properly. Sun and Wen [13] conducted shake table tests to investigate the influence of pile-soil-structure interactions on seismic

responses and dynamic properties of a large-scale model of a cable-stayed bridge and concluded that the SSI effect changes significantly with ground motion frequencies. Fiorentino et al. [14] also conducted shaking table tests to explore the potential benefits stemming from the use of compressible inclusions (CIs) and non-moment resisting pile-to-cap connections in different combinations, with emphasis on SSI. It was found that CI reduces the accelerations on the bridge deck and the settlements in the backfill, while disconnecting piles from the cap decreases bending near the pile head. Tang et al. [15] conducted testing of a long-span bridge based on real-time dynamic input, involving combined use of a shake table array and computational simulations for SSI. It was found that the influence of SSI is closely related to the shear wave velocity in soil. Dai et al. [16] investigated the effect of SSI and isolation pads on the dynamic characteristics of an instrumented bridge using transfer functions, and measured motions in the frequency domain, and concluded that SSI is more significant in the transverse direction than the longitudinal one, and more at the top of the pier than at the deck. Dezi et al. [17] investigated the effects of SSI on the seismic response of an isolated three-span motorway overcrossing equipped with HDRBs, and conducted that SSI may increase deformation and forces on the isolation devices than those of fixed-base models.

The friction pendulum system (FPS) proposed by Zayas et al. [18] is regarded as one of the most effective base isolation systems designed for bridges against dynamic ground motions caused by earthquakes. There are several approaches [19–21] studying the dynamic behaviour and seismic response of isolated bridges equipped with FPS. Recent studies [19, 22, 23] on optimization of friction pendulum bearings had identified the optimal value of the sliding friction coefficient and the isolation period to minimize the vibration amplitude of bridge structures. However, in most of these analyses, the foundation of the isolated bridge was usually assumed rigid, and the flexibility of the supporting soil was neglected. Several other studies such as those of Hassan and Billah [24], Castaldo and Tubaldi [25], Eröz and DesRoches [26] and Yurdakul and Ates [27] indicated that ground motion characteristics can significantly affect the dynamic response of isolated bridges. Clearly, factors of the ground motion and parameters of FPS should be considered together in seismic response analyses with the effect of SSI.

Several studies were found considering SSI of structures equipped with FPS. Krishnamoorthy and Anita [28] did a finite element analysis of an FPS-isolated building structure considering SSI using 2D plane element models with two translational and one rotational degrees of freedom. Ates and Constantinou [29], Wang et al. [30] and Han et al. [31] investigated the seismic response of isolated bridges with friction sliding bearings considering SSI for curved, continuous girder and reinforced concrete single pylon cable-stayed bridges. They showed that isolation systems reduce the shear force and bending moment in the base of reinforced concrete pier effectively, but at the cost of increasing the absolute displacement of the bridge superstructure.

This paper presents a numerical analysis of a 3-span full bridge-pile model for seismic responses of a continuous bridge isolated with FPS, considering SSI using six recorded ground motions during earthquakes. The seismic response of continuous bridge with SSI is compared to those without SSI. Findings of this study can be used to identify the influential factors of SSI on the response amplitude (e.g., displacement, accelerations, shear forces and bending moments) under ground motions, and provide an effective method to study the influence of SSI on the seismic response of different types of bridges.

2. Numerical Model

To investigate the influence of SSI, a numerical model of a continuous bridge with FPS in a five-layered soil deposit was defined and shown in Figure 1(a). The bridge consists of three box beam spans in length of 32 m each, and the bridge deck is from one abutment to the other and is supported by two double circular piers of 1.5 m diameter and 8 m height in between. Each set of the double circular piers is further supported by a 5.8 m by 4 m rectangular pile cap bearing of 2 m height above a group of 12 subpiles of 20 m length and 0.6 m diameter in a 4 by 3 layout. The bridge deck and abutment are connected through expansion joints. The axial view of the main beam-bearing-pier structure is shown in Figure 1(b), with two FPS installed to isolate the main box girder beam. The cross section and dimensions of the main beam, the main pier, the pile cap, the subpile groups are presented in Figures 1(c) to 1(e), respectively.

2.1. Pile-Soil Interaction. The lateral soil resistance-deflection relationship was determined using the *p-y* nonlinear curves following the guidelines of API [8] as given by equations (1) to (4). The equations were used to determine the characteristics of sand and/or soil [10], referred as soil onwards. p_{us} and p_{ud} are the ultimate lateral bearing capacity by the shallow and deep depths, and p_u is the lower value of p_{us} and p_{ud} at depth H. The *p-y* nonlinear curves are obtained according to equtaion (4).

$$p_{us} = (C_1 \times H + C_2 \times D) \times \gamma \times H, \tag{1}$$

$$p_{ud} = C_3 \times D \times \gamma \times H, \tag{2}$$

$$p_u = \min\{p_{us}, p_{ud}\}, \tag{3}$$

$$P = A \times p_u \times \tanh\left[\frac{k \times H}{A \times p_u} \times y\right], \tag{4}$$

where C_1, C_2 and C_3 are the dimensionless coefficients related to the angle Φ of the internal friction of soil, which is given in Table 1. H is the soil layer depth, D the pile diameter, and γ the effective soil weight. A is the factor to account for the cyclic or static loading condition and is selected as 0.9. k is the initial modulus representing the bearing capacity of subgrade, which is related to Φ. y is the lateral deflection of

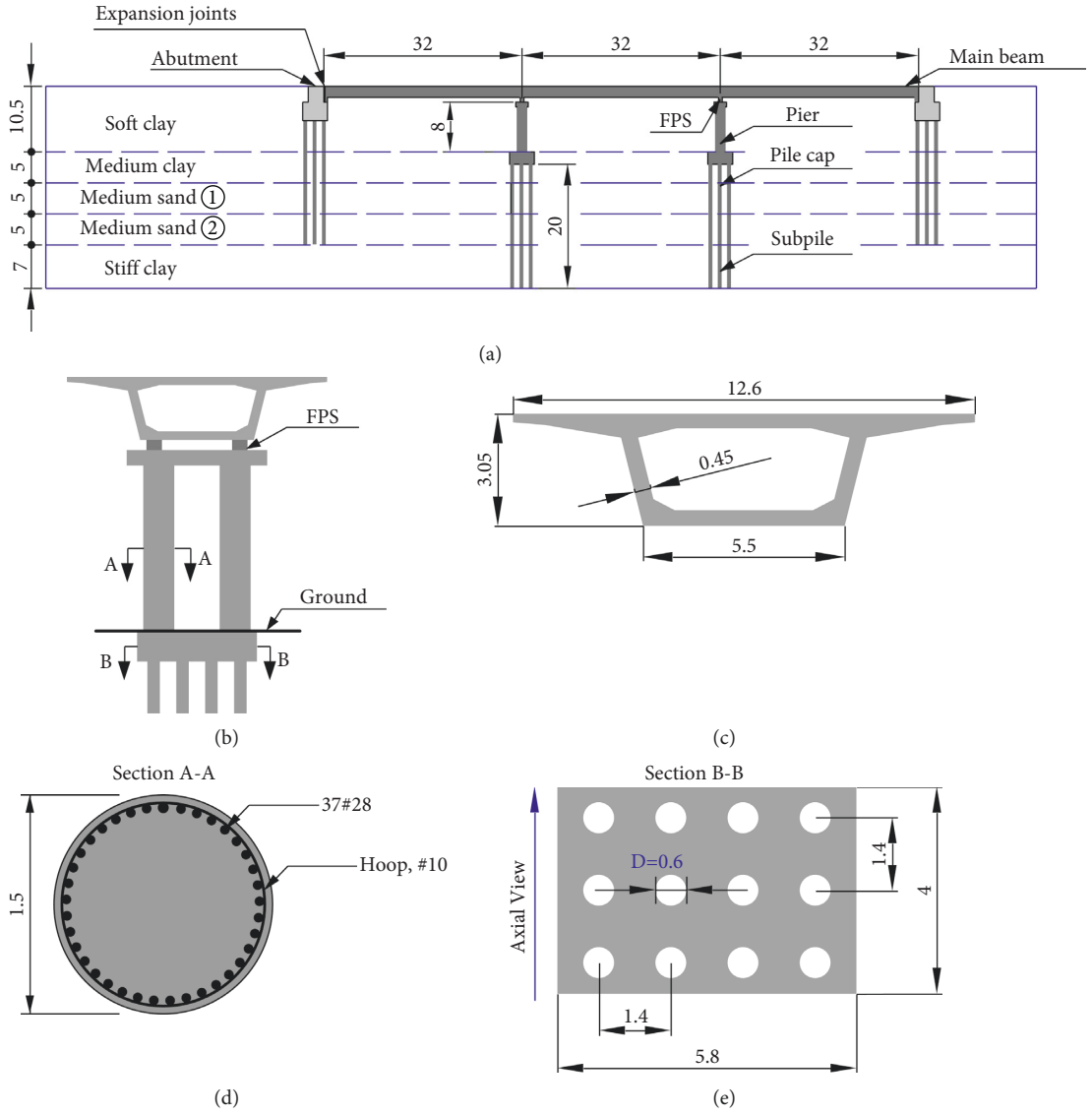

Figure 1: The configuration of typical concrete continuous bridge. (a) Side view of the bridge elevation and four-layer soil profile. (b) Axial view of the bridge structures. (c) Cross section of the main beam. (d) Cross section of a single pier. (e) Cross section of the pile cap and 12 subpiles. Dimensions are in m.

soil. The parameters of the five soil layers in the model are shown in Table 1.

2.2. Ground Motions. To study the ground motion effect, recorded data of six selected earthquakes were used separately as the input to the bridge system. El-Centro (1940), Taft (1952), Northridge (1994), Kobe (1995) and San Fernando (1995) waves are widely used in seismic response analyses [12, 19, 27, 28]. Tianjin [32] wave signal is also included, which was recorded during a major earthquake in China in 1976. Data signals are shown in Figure 2.

Figure 3 shows the acceleration response spectrum of the selected ground motions, the target spectrum is drawn following the Chinese MOT Code [33] for seismic design of highway bridges when the seismic fortification intensity is nine. As can be seen, the response spectrum is not consistent with the target spectrum due to the target acceleration being 0.4 g, corresponding to the target seismic fortification intensity by the design code. So a new acceleration response spectrum was drawn as shown in Figure 4 where the acceleration amplitude of the selected ground motions was scaled to 0.4 g according to the factors given in Table 2. It shows that the characteristic periods of the selected ground motions have a wide range from 0.25 s to 0.95 s.

3. Simulation Results and Discussion

3.1. The FE Model. A three-dimensional finite element model was built for the continuous bridge shown in Figure 1 using SAP2000 [34], a finite element (FE) code commercially available for general structural analyses. The FE model is shown in Figure 5, including abutments, piers and eight FPS

Table 1: Distribution and parameters of soil layers.

Soil type	Soft clay	Medium clay	Medium sand ①	Medium sand ②	Stiff clay
H (m)	10.5	5	5	5	7
γ (kN/m^3)	16.5	17.5	18.5	20.0	20.5
Φ (°)	24	26	30	30	33
C_1	1.06	1.25	1.92	1.98	2.55
C_2	1.91	2.10	2.64	2.81	3.17
C_3	14	16	28	30	42
k (kN/m^3)	3200	4000	15000	17000	28000

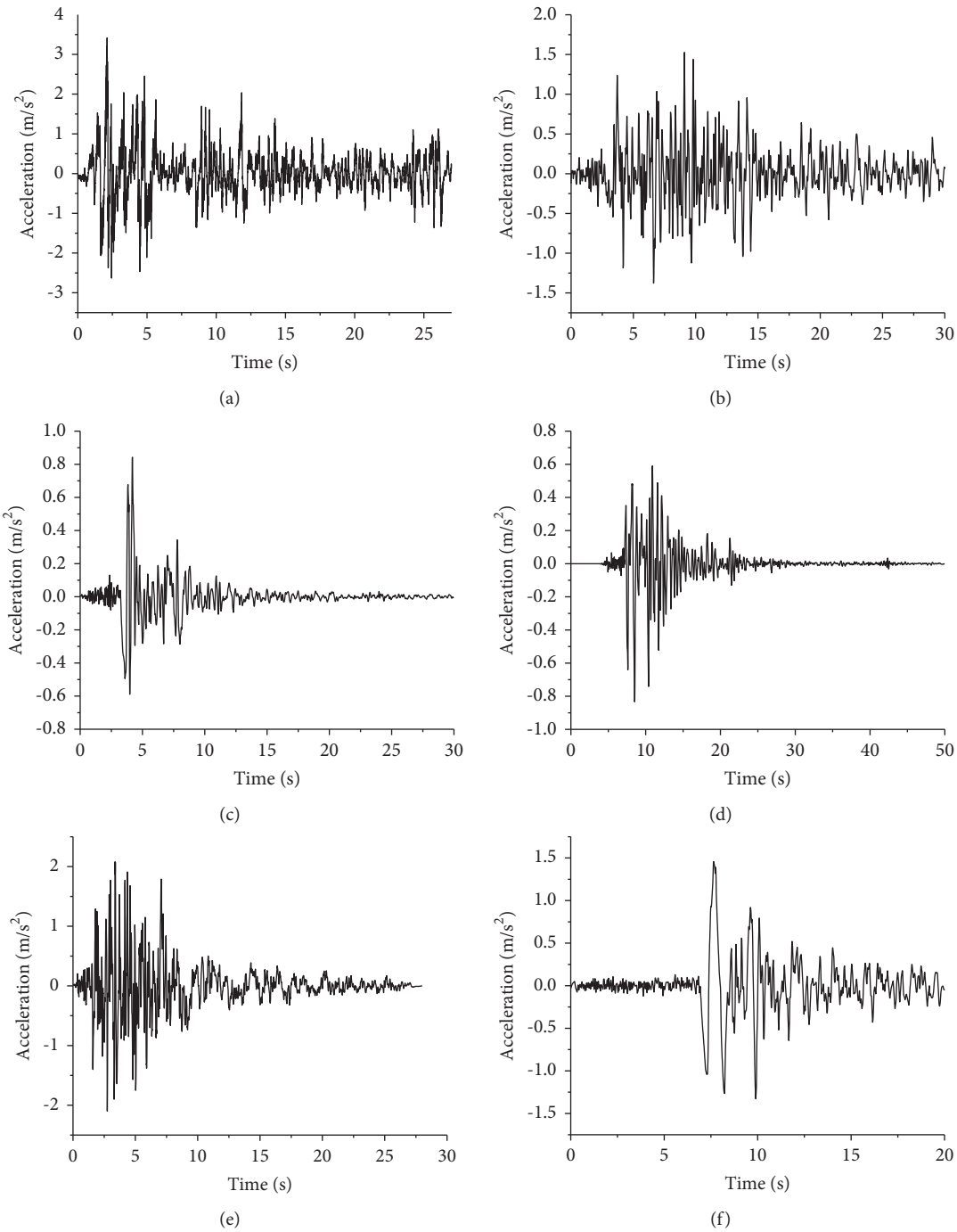

Figure 2: Acceleration time histories of input ground motions. (a) El-Centro wave. (b) Taft wave. (c) Northridge wave. (d) Kobe wave. (e) San Fernando wave. (f) Tianjin wave.

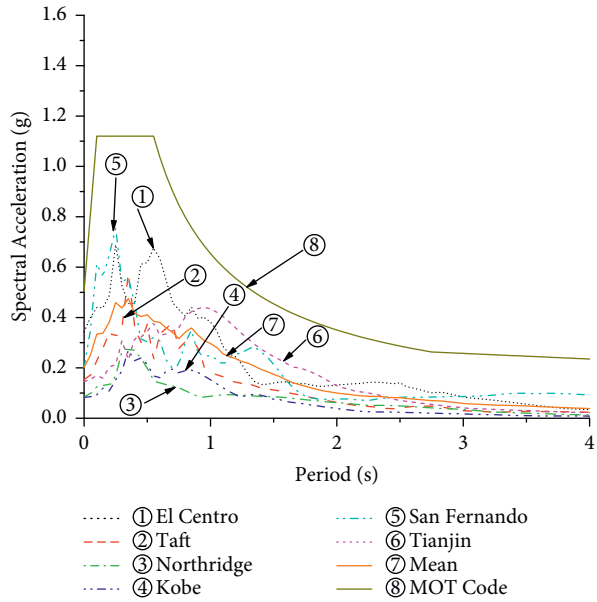

Figure 3: Acceleration response spectrum of the selected ground motions.

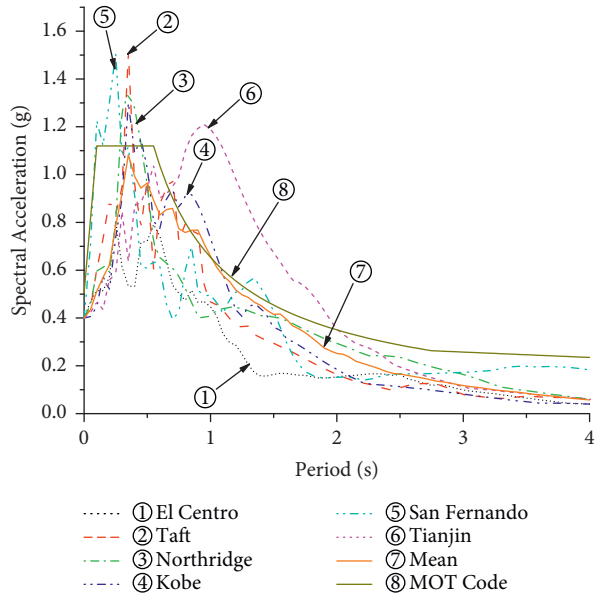

Figure 4: Acceleration response spectrum of the selected ground motions scaled for acceleration of 0.4 g.

Table 2: Scale factors used to scale the ground motions.

Ground motion	ElCentro	Taft	Northridge	Kobe	San Fernando	Tianjin
Scale factors	1.17	2.62	4.75	4.80	1.91	2.74

units. Beam elements provided by the FE code were used for the main box beams, piers and subpiles. Mid-thick shell elements were used for the pile caps and abutments. All material parameters were set according to design specifications. The frictional function of FPS was modelled by the friction isolator available in the code, which is a nonlinear element with a friction coefficient, using the spherical radius of the contact surfaces and the vertical stiffness as the defined parameters. Soil was modelled as springs by the nonlinear link-element (following the p-y curve) which can simulate pile-soil interactions according to the theoretical calculation parameters using equation (4). Expansion joints were modelled as linear springs. Convergence tests of the FE model were carried out for the appropriate mesh density.

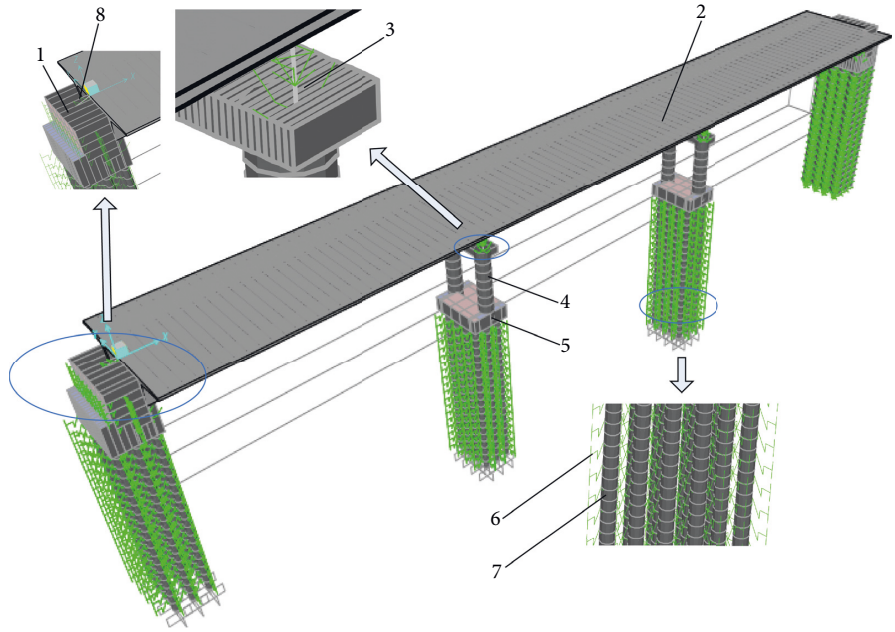

Figure 5: The finite element model of a three-span continuous bridge with FPS and structure-soil interaction. (1) Abutment; (2) main beam; (3) FPS; (4) pier; (5) pile cap; (6) soil; (7) subpile; (8) expansion joints.

Table 3: Comparison of the modal periods under different radii of FRS.

FRS radius (m)		Bridge vibration modes					
		1	2	3	4	5	6
1	FEA with SSI	2.20	2.17	1.65	0.24	0.23	0.22
	FEA without	2.15	2.14	1.64	0.25	0.17	0.16
	Difference	2.32%	1.40%	0.61%	4.00%	35.3%	37.5%
2	FEA with SSI	3.03	3.01	2.30	0.25	0.24	0.22
	FEA without	3.00	2.99	2.26	0.26	0.17	0.16
	Difference	1.00%	0.67%	1.77%	3.85%	41.2%	37.5%
3	FEA with SSI	3.72	3.70	2.84	0.25	0.24	0.22
	FEA without	3.69	3.68	2.64	0.26	0.17	0.16
	Difference	0.81%	0.54%	7.58%	3.85%	41.2%	37.5%
4	FEA with SSI	4.18	4.16	3.23	0.26	0.25	0.22
	FEA without	4.15	4.15	3.20	0.26	0.17	0.16
	Difference	0.72%	0.24%	0.94%	0%	47.1%	37.5%

3.2. Modal Analysis. Table 3 shows simulated results with and without the influence of SSI on the modal periods of the first six vibration modes, and the corresponding differences, when the FRS radius was set as 1 m, 2 m, 3 m and 4 m, respectively.

Modes 1, 2 and 3 are in the transverse, longitudinal and cross section rotational directions of the bridge, respectively. The theoretical 1st isolation period of the bridge, Tp, was given by equation (5) [20, 35]:

$$T_p = 2\pi\sqrt{\frac{R}{g}}, \tag{5}$$

where R is the radius of the spherical concave surface of FPS, g is the acceleration of gravity. Equation (5) shows T_p is only related to R, irrespective whether SSI is considered or not.

From equation (5), the isolation periods of mode 1 are 2.01 s, 2.84 s, 3.74 s and 4.01 s corresponding to the FRS radius at 1 m, 2 m, 3 m and 4 m, respectively. As can be observed, simulated 1st mode periods are very close to the theoretical ones with errors in the range of 0.54% to 8.6% for both cases of with and without considering SSI. This indicates that SSI might be regarded as having a negligible influence on the first modes of the isolated bridge.

For high modes, there is no theoretical solution. Table 3 and Figure 6 show little difference for modes 2 to 4 between simulated results with and without SSI, indicating an insignificant effect of SSI and a significant one of FRS radius in a monotonically increasing trend. In comparison, for higher modes 5 and 6, a more prominent influence of SSI can be viewed in Table 3 and Figure 7, with little influence by FRS radii.

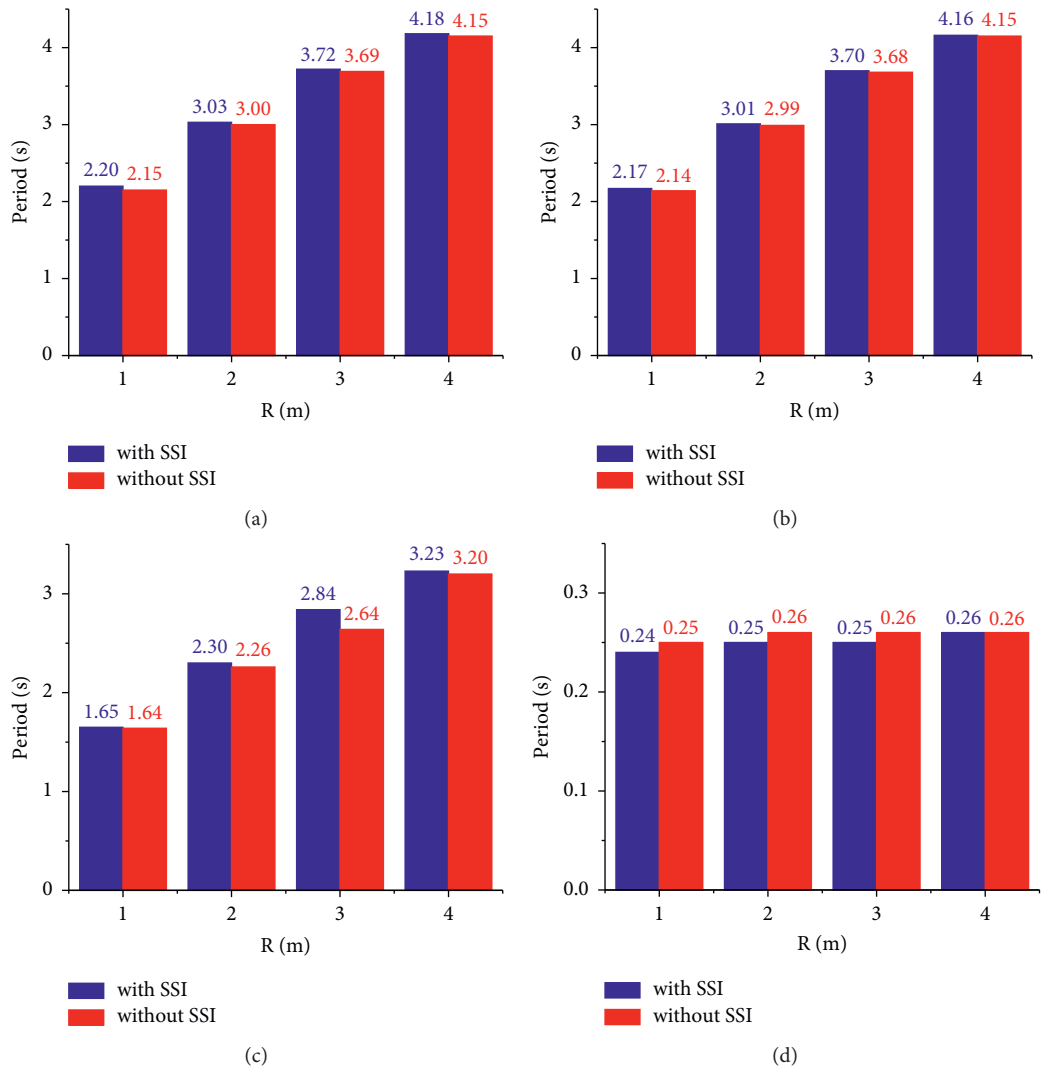

Figure 6: Periods of modes 1 to 4 under different radii of FRS. (a) Mode 1. (b) Mode 2. (c) Mode 3. (d) Mode 4.

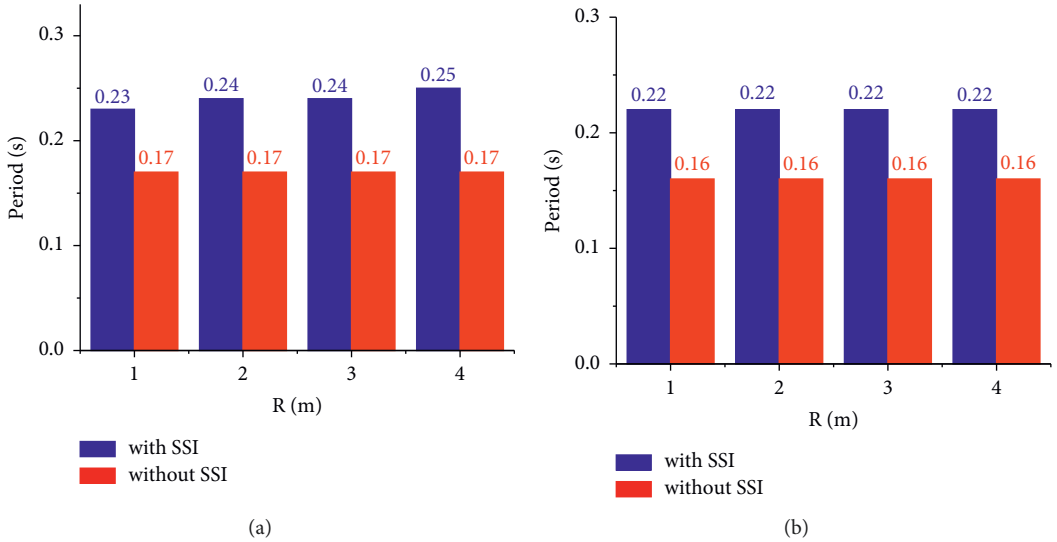

Figure 7: Periods of modes 5 to 6 under different radii of FRS. (a) Mode 5. (b) Mode 6.

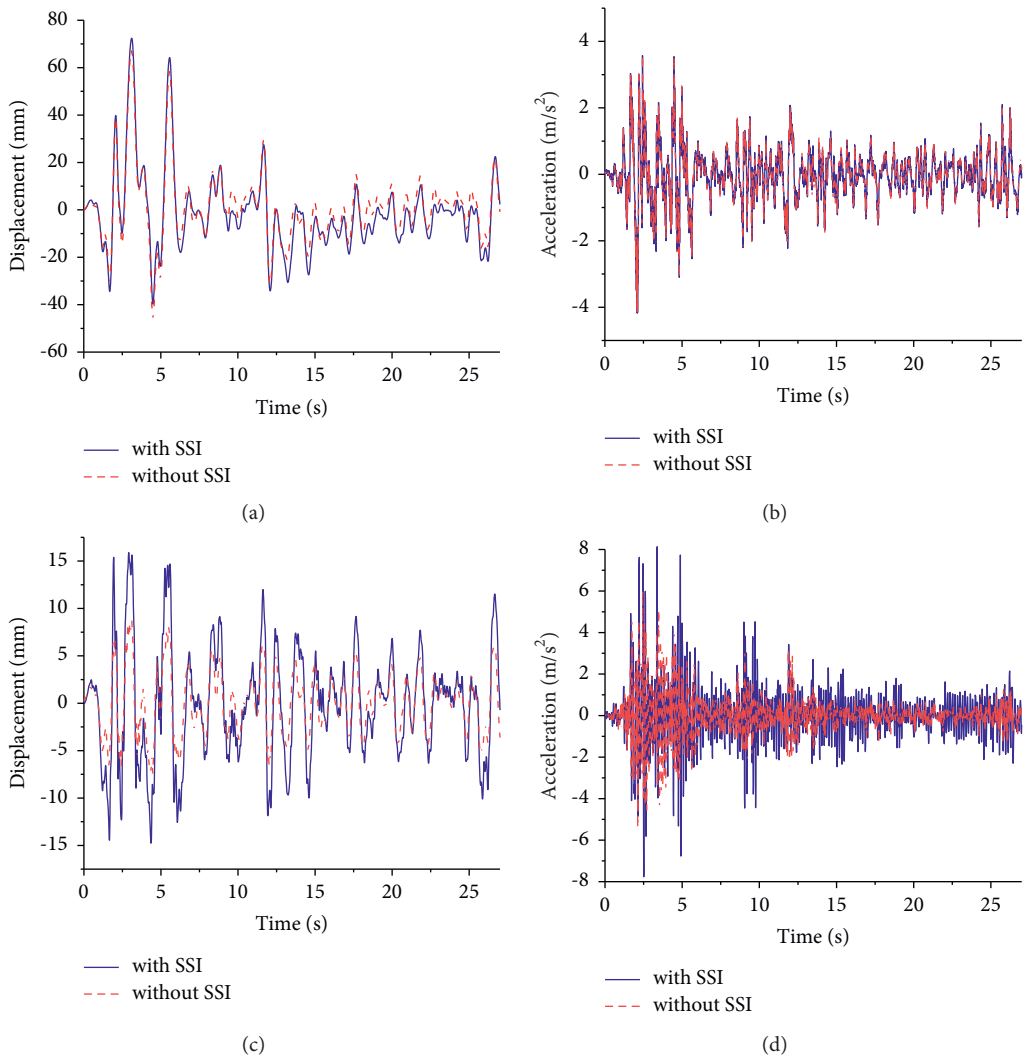

Figure 8: Comparison of the dynamic responses of the main beam and the pier top under ElCentro wave. (a) Displacement of the main beam. (b) Acceleration of the main beam. (c) Displacement of the pier top. (d) Acceleration of the pier top.

3.3. Influence of SSI on the Dynamic Response of the Isolated Bridge. In the following sections, simulated results using the EI Centro wave as the seismic input are shown to illustrate the dynamic response of the isolated bridge with and without SSI. The sliding friction coefficient of FPS was set at 0.05.

Figures 8(a) and 8(b) show the time history of the displacement and acceleration of the main beam with and without SSI. As can be seen, the influence of SSI on the main beam is very limited. But the influence of SSI is more significant on the pier top as shown in Figures 8(c) and 8(d) where the magnitude of the displacement and acceleration is increased significantly when SSI is considered.

Figures 9(a) and 9(b) show the time response of the shear force and the bending moment at the pier bottom with and without SSI. Both are reduced significantly when SSI is considered. Figures 9(c) and 9(d) show the displacement and acceleration at the pier bottom with SSI. Due to the fixed constraints at the pier bottom when SSI is not considered, the displacement and acceleration are both zero.

3.4. Influence of the Friction Coefficient on the Bridge Response Amplitude. Figures 10–12 illustrate the influence of SSI in terms of the friction coefficient of FPS. The El Centro wave was again considered as the input.

The equivalent stiffness of FPS increases with the increase of the friction coefficient [17], leading to reduced displacement but increased acceleration of the main beam as shown in Figures 10(a) and 10(b), respectively. It can also be seen that the reduction on the displacement is more effective when the friction coefficient is less than 0.04. Further increase of the coefficient appears to have little influence on the displacement. In comparison, the increase of the acceleration of the main beam is approximately linear. SSI also appears to have no effect at all.

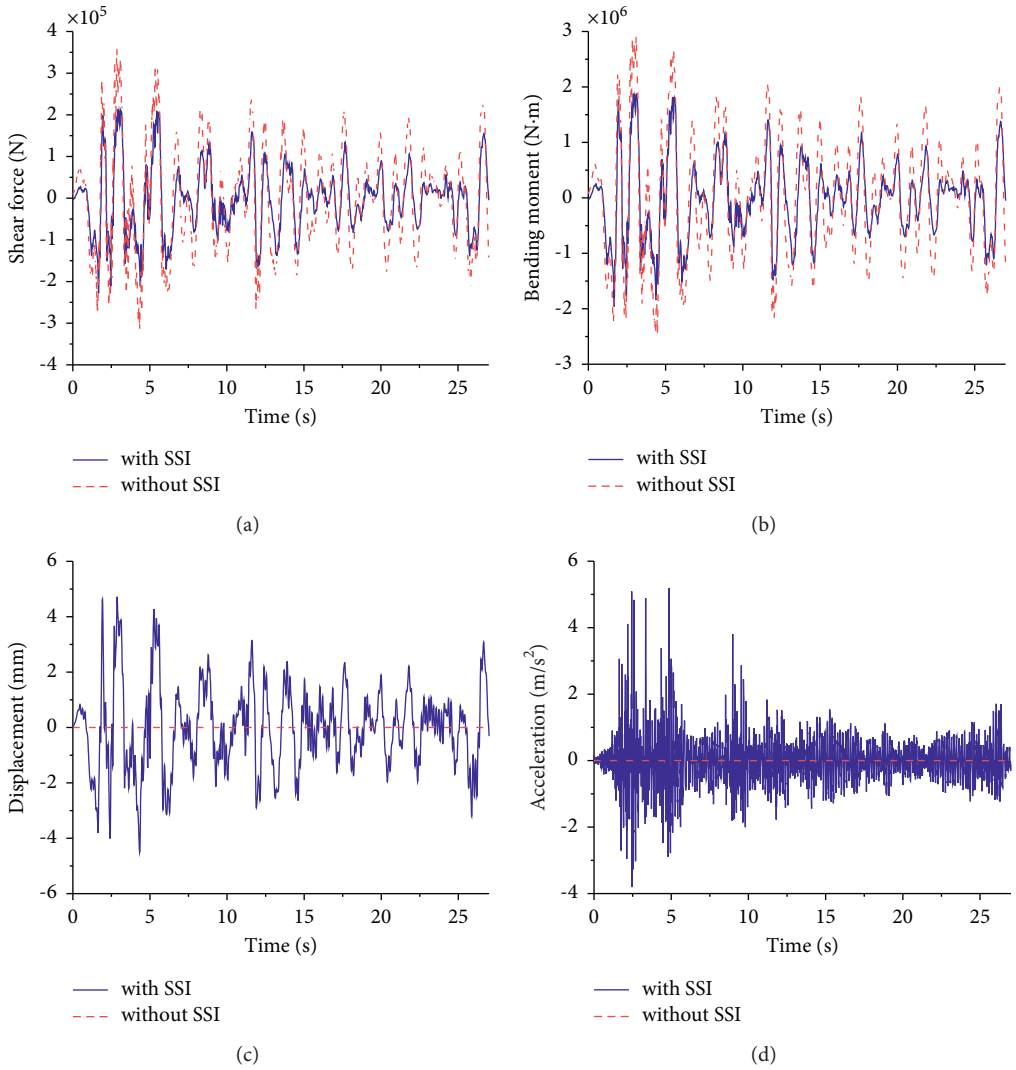

Figure 9: Comparison of the dynamic responses of the pier bottom under ElCentro wave. (a) Shear force at the pier bottom. (b) Bending moment at the pier bottom. (c) Displacement at the pier bottom. (d) Acceleration at the pier bottom.

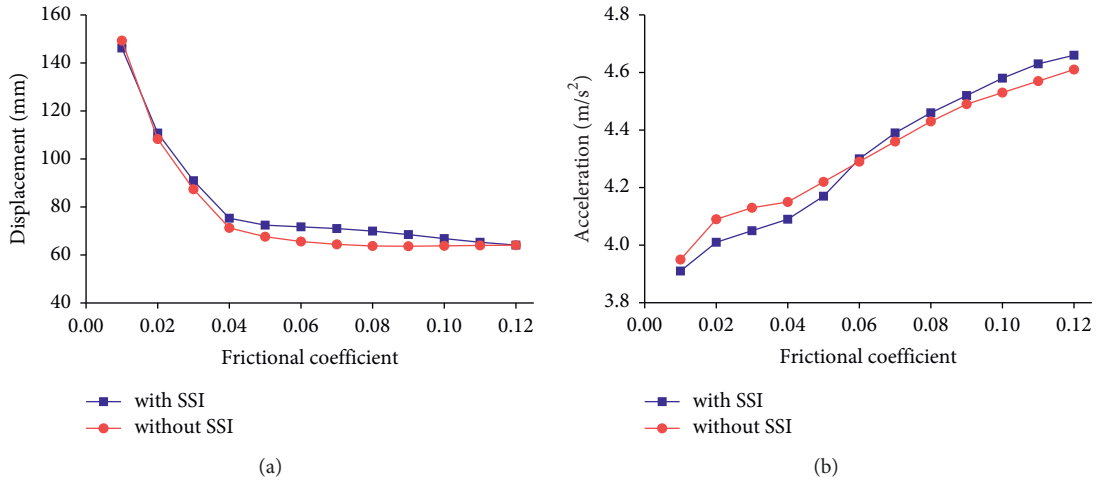

Figure 10: Comparison of the response amplitude of the main beam over the friction coefficient of FPS under ElCentro wave. (a) Displacement of the main beam. (b) Acceleration of the main beam.

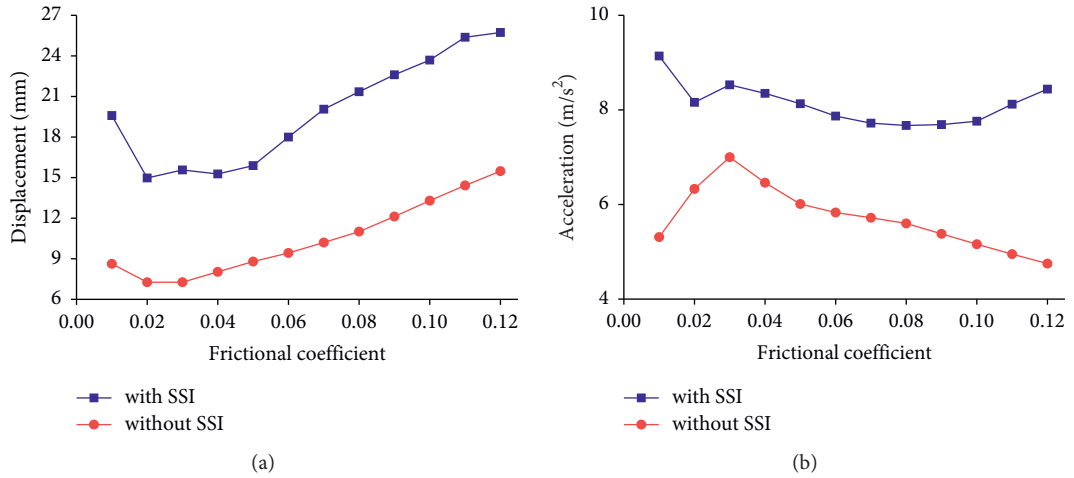

FIGURE 11: Comparison of the response amplitude of the pier top over the friction coefficient of FPS under ElCentro wave. (a) Displacement of the pier top. (b) Acceleration of the pier top.

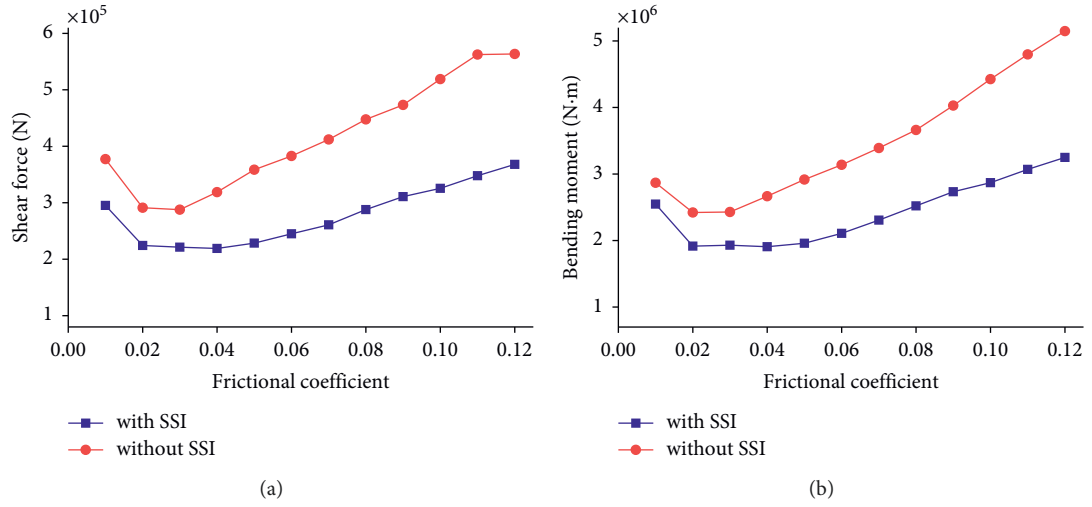

FIGURE 12: Comparison of the response amplitude of the pier bottom over the friction coefficient of FPS under ElCentro wave. (a) Shear force of the pier bottom. (b) Bending moment of the pier bottom.

Figure 11 illustrates the displacement and acceleration of the pier top in terms of the friction coefficient of FPS with and without SSI. Displacements decrease first then increase when the friction coefficient is around 0.02–0.03. Accelerations with SSI also decrease before coefficient being 0.02, then remain barely variable afterwards. In contrast, accelerations without SSI increase first until 0.03 then decrease approximately in a linear pattern. The magnitude of both the displacement and acceleration is increased significantly when SSI is considered than not.

For the shear forces and moment at the pier bottom, Figure 12 shows similar patterns for both in terms of the friction coefficient, with reduction first until the coefficient is around 0.02–0.03 then increase monotonically. Consideration with SSI reduces the magnitude of both the shear force and bending moment significantly over the whole range of the friction coefficient considered.

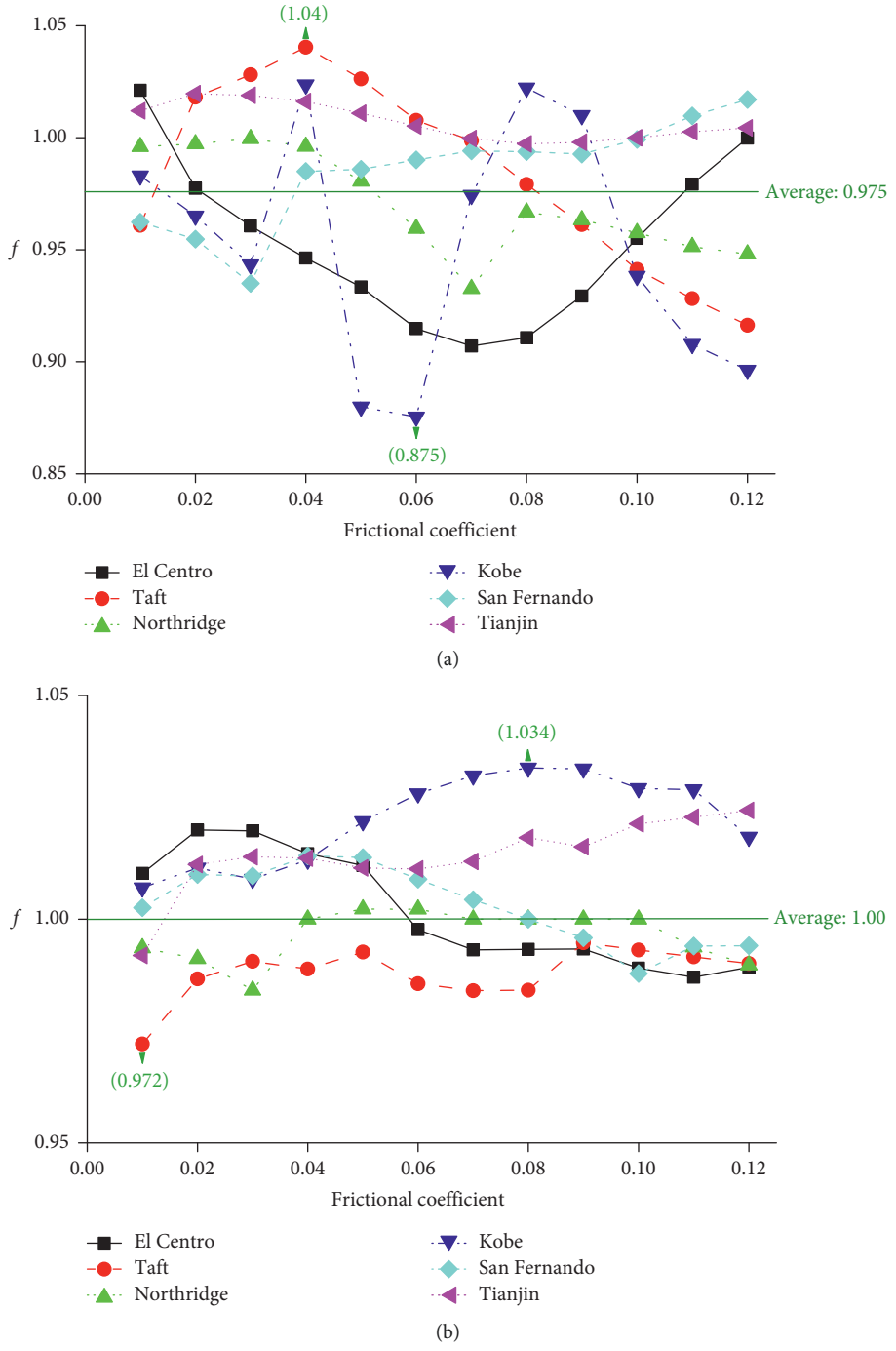

Figure 13: Comparison of the response amplitude of the main beam under various ground motions. (a) Displacement amplitude of the main beam. (b) Acceleration amplitude of the main beam.

3.5. Influence of SSI on the Response Amplitudes under Various Ground Motions. To compare the impacts of SSI under the six ground motions considered, the ratio of the response amplitudes without and with SSI was calculated to reveal the relative difference between the two, f = response without SSI/ Response with SSI.

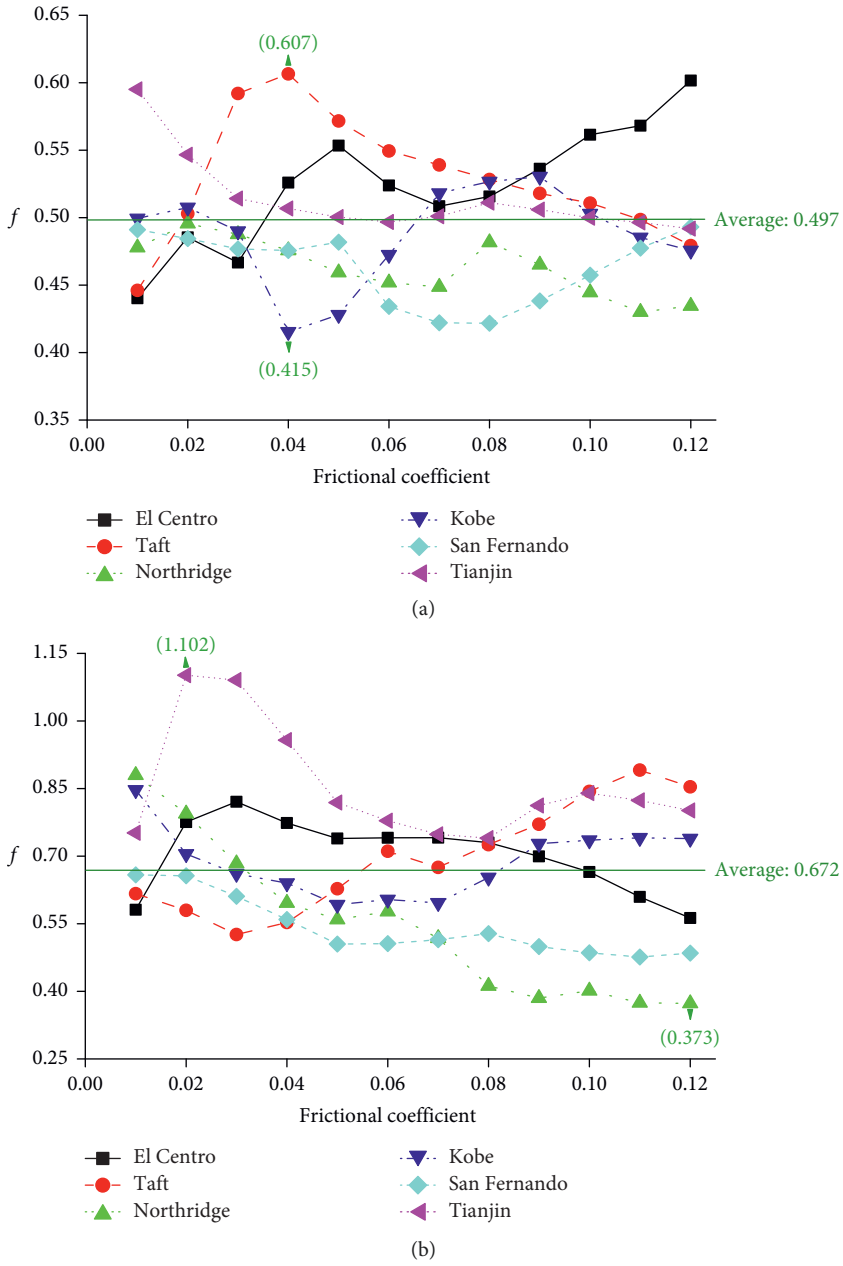

Figure 14: Comparison of the response amplitude of the pier top under various ground motions. (a) Displacement amplitude of the pier top. (b) Acceleration amplitude of the pier top.

An f value bigger than one indicates a "reduction" by SSI.

Values of f for the considered ground motions are shown in Figures 13–15 in terms of the frictional coefficient of FPS.

Figures 13(a) and 13(b) give f of the displacement and acceleration of the main beam, showing moderate influence of SSI on the displacement (0.875–1.04), and very limited on the acceleration (0.972–1.034). Overall, the influence of SSI on the response of the main beam is broadly negligible.

Figures 14(a) and 14(b) give f of the displacement and acceleration of the pier top, showing the displacement amplitude at the pier top with SSI is constantly smaller than without (0.415–0.607), and the acceleration amplitude with SSI is also broadly reduced than without except for individual points (0.373–1.102).

Figures 15(a) and 15(b) illustrate f of the shear force and bending moment at the pier bottom. As can be seen, the influence of SSI is equally significant on both the

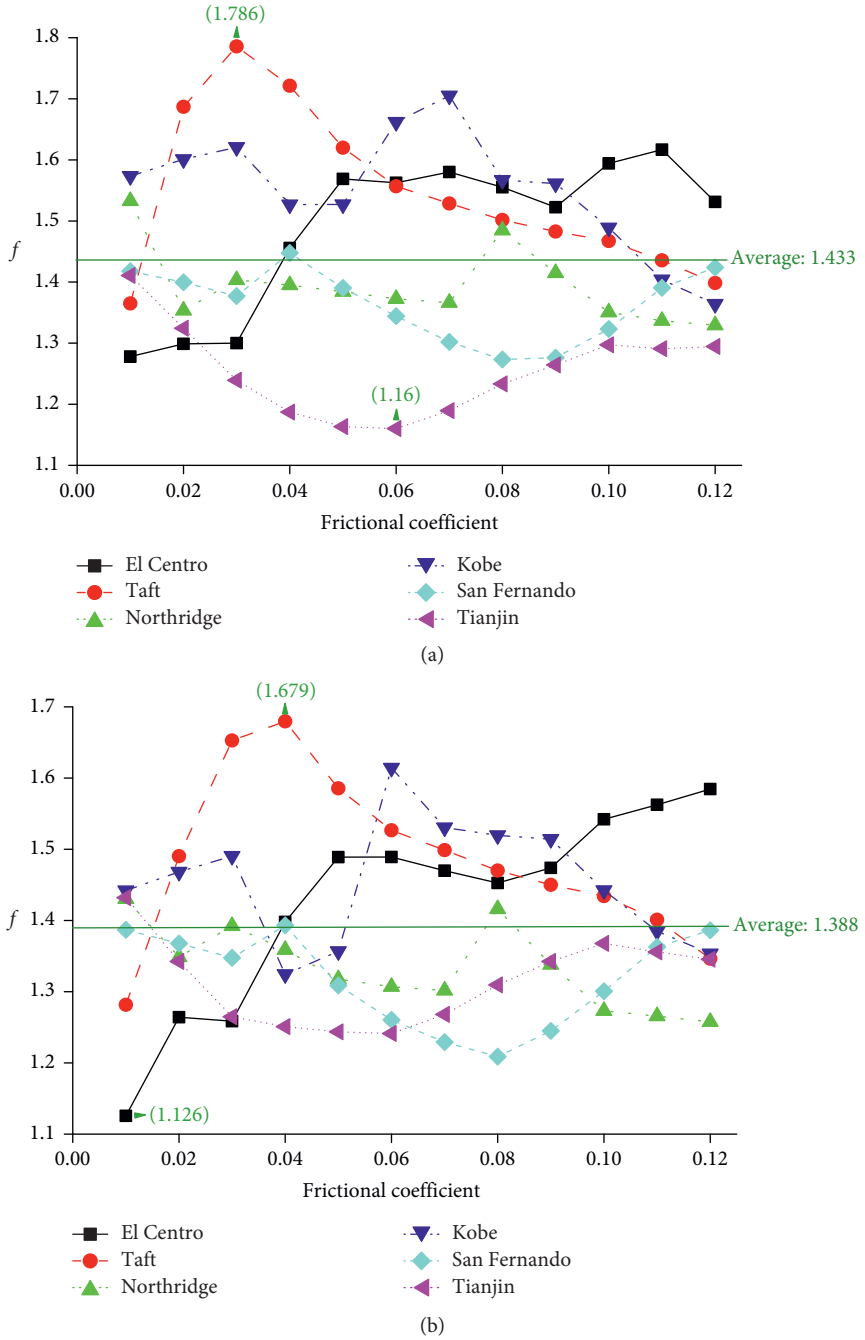

Figure 15: Comparison of the response amplitude of the pier bottom under various ground motions. (a) Shear force of the pier bottom. (b) Bending moment of the pier bottom.

shear force (1.16–1.786) and the moment (1.126–1.679) with the magnitude reduced significantly when SSI is considered.

4. Conclusions

A finite element analysis was carried out on a three-span continuous bridge with FPS, considering SSI modelled by nonlinear springs following the *p-y* curve under several measured ground motions. Based on the outcome, the following observations can be drawn for the seismic analysis of continuous bridge.

It is remarkable that, SSI has a negligible effect on the period of lower vibration modes of FPS-isolated bridges (eg. the first four modes), but increases the period of higher modes. It is noticed that the periods of the first three vibration modes increase in terms of the FPS radius, and the periods of higher modes are influenced by the radius.

It is also observed that the acceleration of the main beam is less affected by SSI, but is more obvious on the

displacement, and the shear force and bending moment at the pier bottom are both significantly influenced by SSI for all ground motions and friction coefficients considered, with the magnitude reduced at the range from 12.6% to 78.6% when SSI is considered.

It should be noted that an optimal value of the friction coefficient exists for FRS at around 0.03 where the bridge response to ground motions such as the displacement acceleration, shear and moment are at the minimum. Further increase of the coefficient value appears to be detrimental. This will be a useful guideline for design and surely warrants for further investigation in future studies.

Data Availability

Some or all data, models, or code that support the findings of this study are available from the corresponding author upon reasonable request.

Conflicts of Interest

The authors declare that they have no conflicts of interest.

Acknowledgments

This study was supported by the Doctoral Scientific Research Foundation of North China University of Water Resources and Electric Power, the Key Research Projects of Higher Education Institutions in HENAN (20A450002), and the Science and Technology Projects of Henan Province (222102320084).

References

[1] V. Anand and S. R. Satish Kumar, "Seismic soil-structure interaction: a state-of-the-art review," *Structures*, vol. 16, pp. 317–326, 2018.

[2] A. Dehghanpoor, D. Thambiratnam, E. Taciroglu, and T. Chan, "Soil-pile- superstructure interaction effects in seismically isolated bridges under combined vertical and horizontal strong ground motions," *Soil Dynamics and Earthquake Engineering*, vol. 126, p. 15, Article ID 105753, 2019.

[3] X. Z. Li, X. B. Liu, and D. J. Liu, "Coupled vibration analysis of a railway continuous rigid-frame bridge and vehicles with soil-structure interaction," *Journal of Shock and Vibration*, vol. 20, no. 12, pp. 54–58, 2011, (in Chinese).

[4] M. Novak and H. Mitwally, "Transmitting boundary for axisymmetrical dilation problems," *Journal of Engineering Mechanics*, vol. 114, no. 1, pp. 181–187, 1988.

[5] M. Priestley, F. Seible, and G. M. Calvi, *Seismic Design and Retrofit of Bridges*, Wiley, New York, NY, USA, 1996.

[6] M. Dicleli and M. Y. Mansour, "Seismic retrofitting of highway bridges in Illinois using friction pendulum seismic isolation bearings and modeling procedures," *Engineering Structures*, vol. 25, no. 9, pp. 1139–1156, 2003.

[7] A. Rahmani, M. Taiebat, W. D. Liam Finn, and C. E. Ventura, "Evaluation of substructuring method for seismic soil-structure interaction analysis of bridges," *Soil Dynamics and Earthquake Engineering*, vol. 90, pp. 112–127, 2016.

[8] Api (American Petroleum Institute), *Recommended Practice for Planning, Designing, and Constructing Fixed Offshore Platforms. Section 6.8 Soil Reaction for Laterally Loaded Piles*, American Petroleum Institute, Washington, DC, USA, 2007.

[9] Z. H. Wang, L. Duenas-Osorio, and J. E. Padgett, "Influence of soil-structure interaction and liquefaction on the isolation efficiency of a typical multispan continuous steel girder bridge," *Journal of Bridge Engineering*, vol. 19, no. 8, pp. 1–12, 2014.

[10] Q. Han, J. Y. Chen, X. L. Du, and C. Huang, "Nonlinear seismic response of skewed highway bridges subjected to bidirectional near-fault ground motions," *Journal of Bridge Engineering*, vol. 22, no. 7, pp. 1–14, 2014.

[11] B. B. Soneji and R. S. Jangid, "Influence of soil-structure interaction on the response of seismically isolated cable-stayed bridge," *Soil Dynamics and Earthquake Engineering*, vol. 28, no. 4, pp. 245–257, 2008.

[12] S. Mahjoubi and S. Maleki, "Finite element modelling and seismic behaviour of integral abutment bridges considering soil-structure interaction," *European Journal of Environmental and Civil Engineering*, vol. 24, no. 6, pp. 767–786, 2020.

[13] L. M. Sun and X. Wen, "Evaluation of pile-soil-structure interaction effects on the seismic responses of a super long-span cable-stayed bridge in the transverse direction: a shaking table investigation," *Soil Dynamics and Earthquake Engineering*, vol. 125, pp. 245–257, 2019.

[14] G. Fiorentino, C. Cengiz, F. De Luca et al., "Integral abutment bridges: investigation of seismic soil-structure interaction effects by shaking table testing," *Earthquake Engineering & Structural Dynamics*, vol. 50, no. 6, pp. 1517–1538, 2021.

[15] Z. Y. Tang, H. Ma, J. Gao, and Z. B. Li, "Effect of soil-structure interaction on seismic performance of long-span bridge tested by dynamic substructuring method," *Shock and Vibration*, vol. 2017, Article ID 4358081, 12 pages, 2017.

[16] W. T. Dai, F. Rojas, C. Shi, and Y. Tan, "Effect of soil structure interaction on the dynamic responses of base isolated bridges and comparison to experimental results," *Soil Dynamics and Earthquake Engineering*, vol. 114, pp. 245–252, 2018.

[17] F. Dezi, S. Carbonari, A. Tombari, and G. Leoni, "Soil-structure interaction in the seismic response of an isolated three span motorway overcrossing founded on piles," *Soil Dynamics and Earthquake Engineering*, vol. 41, pp. 151–163, 2012.

[18] V. A. Zayas, S. S. Low, and S. A. Mahin, "A simple pendulum technique for achieving seismic isolation," *Earthquake Spectra*, vol. 6, no. 2, pp. 317–333, 1990.

[19] A. Saha, P. Saha, and S. K. Patro, "Polynomial friction pendulum isolators (PFPIs) for seismic performance control of benchmark highway bridge," *Earthquake Engineering and Engineering Vibration*, vol. 16, no. 4, pp. 827–840, 2017.

[20] B. Li, B. Wang, S. H. Wang, and X. Wu, "Energy response analysis of continuous beam bridges with friction pendulum bearing by multihazard source excitations," *Shock and Vibration*, vol. 2020, Article ID 3724835, 19 pages, 2020.

[21] Y. P. Wang, L. L. Chung, and W. H. Liao, "Seismic response analysis of bridges isolated with friction pendulum bearings," *Earthquake Engineering & Structural Dynamics*, vol. 27, no. 10, pp. 1069–1093, 1988.

[22] P. Castaldo, M. Ripani, and R. L. Priore, "Influence of soil conditions on the optimal sliding friction coefficient for isolated bridges," *Soil Dynamics and Earthquake Engineering*, vol. 111, pp. 131–148, 2018.

[23] J. Wen, Q. Han, and X. Du, "Shaking table tests of bridge model with friction sliding bearings under bi-directional earthquake excitations," *Structure and Infrastructure Engineering*, vol. 15, no. 9, pp. 1264–1278, 2019.

[24] A. L. Hassan and A. Billah, "Influence of ground motion duration and isolation bearings on the seismic response of base-isolated bridges," *Engineering Structures*, vol. 222, pp. 111–129, 2020.
[25] P. Castaldo and E. Tubaldi, "Influence of ground motion characteristics on the optimal single concave sliding bearing properties for base-isolated structures," *Soil Dynamics and Earthquake Engineering*, vol. 104, pp. 346–364, 2018.
[26] M. Eröz and R. DesRoches, "The influence of design parameters on the response of bridges seismically isolated with the friction pendulum system (FPS)," *Engineering Structures*, vol. 56, pp. 585–599, 2013.
[27] M. Yurdakul and S. Ates, "Stochastic responses of isolated bridge with triple concave friction pendulum bearing under spatially varying ground motion," *Structural Engineering & Mechanics*, vol. 65, no. 6, pp. 771–784, 2018.
[28] A. Krishnamoorthy and S. Anita, "Soil-structure interaction analysis of a FPS-isolated structure using finite element model," *Structures*, vol. 5, pp. 44–57, 2016.
[29] S. Ates and M. C. Constantinou, "Example of application of response history analysis for seismically isolated curved bridges on drilled shaft with springs representing soil," *Soil Dynamics and Earthquake Engineering*, vol. 31, no. 3, pp. 334–350, 2011.
[30] B. F. Wang, Q. Han, and J. F. Jia, "Seismic response analysis of isolated offshore bridge with friction sliding bearing," *Earthquake and Structures*, vol. 16, no. 6, pp. 641–654, 2019.
[31] Q. Han, J. Wen, X. Du, Z. Zhong, and H. Hao, "Nonlinear seismic response of a base isolated single pylon cable-stayed bridge," *Engineering Structures*, vol. 175, pp. 806–821, 2018.
[32] X. Han, P. Y. Ji, Q. C. Gu, and G. S. Mu, "Model test study on dynamic response of expressway plastic-reinforced earth embankment under earthquake," *Geofluids*, vol. 2021, Article ID 5551699, 12 pages, 2021.
[33] Mot (Ministry of Transport), *Specifications for Seismic Design of Highway Bridges*, Ministry of Transport, Beijing, China, 2020.
[34] *SAP2000, Computers and Structures, 1646 N. California Boulevard Suite 600, Walnut Creek, CA, USA*, 2020.
[35] S. Ates and M. C. Constantinou, "Example of application of response spectrum analysis for seismically isolated curved bridges including soil-foundation effects," *Soil Dynamics and Earthquake Engineering*, vol. 31, no. 4, pp. 648–661, 2011.